International Journal of Development Mathematics Vol 2 Issue 4, 283–301

INTERNATIONAL JOURNAL OF DEVELOPMENT MATHEMATICS

ISSN: 3026-8656 (Print) | 3026-8699 (Online)

journal homepage: https://ijdm.org.ng/index.php/Journals

Existence, Persistence and Stability of Periodic Solutions of a Seasonally Forced West Nile Virus Model with Lateral Hosts and Vertical Vector Transmission

Kabiru A. Manju[a*], Abdulfatai A. Momoh[b] and Salaudeen Yusuf [c]

[a]Department of General Studies Education, Federal College of Education, Yola, Adamawa State, Nigeria.

[b]Department of Mathematics, Modibbo Adama University, Yola, Adamawa State, Nigeria.

[c]Department of Epidemiology and Biostatistics, Federal University of Health Sciences, Azare, Bauchi State, Nigeria.

ARTICLE INFO

Article history:

Received: 5 September, 2025

Received in Revised: 20 November, 2025

Accepted: 29 November, 2025

Keywords

West Nile virus, Periodic solution, Basic reproduction ratio, Bird seeding index, Global stability.

Abstract

West Nile virus persists in tropical settings where temperature drives vector development, birds transmit laterally through predation, scavenging and a contaminated environment, and mosquitoes transmit vertically to their progeny. We analyse a twenty-two compartment, seasonally forced model of such transmission in which corvid and non-corvid reservoirs, the full mosquito life cycle, three human infection outcomes and an environmental viral reservoir are coupled through temperature-dependent vital and transmission rates of period one year. Existence of a positive periodic solution is established by Mawhin's continuation theorem after uniform a priori bounds are derived for every compartment; the non-negative orthant is positively invariant, the periodic solution strictly positive, and all trajectories ultimately bounded within a compact absorbing set on which the periodic solution is unique. Setting the avian introduction terms to zero yields a unique disease-free periodic solution, and the periodic reproduction ratio is obtained as the spectral radius of the next-infection operator. Reduction of the thirteen-dimensional next-generation kernel to a five-dimensional block-triangular matrix separates an autonomous human block from a temperature-driven vector-reservoir block. Numerical evaluation gives a threshold of 1.494471, which seasonal forcing depresses well below the constant-temperature value, while a positive bird seeding index sustains transmission below threshold. The endemic periodic orbit is globally asymptotically stable.

*Corresponding author Tel: +234 8035368528

Email address: manjuka@fceyola.edu.ng

https://doi.org/10.62054/ijdm/0204.26

1 Introduction

West Nile virus (WNv) is a vector-borne arbovirus of the flavivirus genus, first isolated by Smithburn et al. (1940) in the West Nile district of Uganda and spread mainly by mosquitoes of the *Culex* genus. It is the most pervasive neuroinvasive arboviral illness worldwide (Ciota and Kramer, 2013), severe cases being life threatening in immuno-compromised, younger and elderly individuals (Kramer et al., 2007). The disease has spread from Africa to Europe, the Americas, the Middle East and West Asia (WHO, 2017) and is becoming endemic in several regions (Sule et al., 2018; Habarugira et al., 2020), with 86,758 verified cases between 1999 and 2023, a figure understated by under-reporting (CDC, 2024c; Ronka et al., 2021).

The major transmission cycle is bird–mosquito–bird. Birds are the primary reservoir (CDC, 2024e), their migration and commercial transportation driving global spread (Chatterjee et al., 2008; Powell and Tabachnick, 2013), and the avian population is commonly divided into a more competent and a less competent category (WOAH, 2024; CWHL, 2024). Lateral avian transmission through predation and scavenging (Komar et al., 2003; Nemeth and Kunkel, 2024; NPS, 2025) and vertical transmission within the vector (Miller et al., 2000; Dohm et al., 2002; Anderson et al., 2014; Nelms et al., 2013) are both documented, and temperature governs mosquito biology and transmission viability (García-Carrasco et al., 2022; ECDPC, 2025; Ciota et al., 2014; Mordecai et al., 2019; Heidecke et al., 2025). Humans are dead-end hosts (Clark and Schaefer, 2023) but transmit among themselves through organ transplant (CDC, 2024d; Kusne and Smilack, 2005; Kumar et al., 2004), blood transfusion (Jimenez et al., 2021) and, rarely, breast feeding (Hinckley et al., 2007; Stobierski et al., 2002).

Existing models treat these mechanisms separately: mosquito–bird invasion analysis (Wonham et al., 2004; Cruz-Pacheco et al., 2005), control strategies (Bowman et al., 2005), backward bifurcation and optimal control (Blayneh et al., 2010; Abdelrazec et al., 2015), spatial spread and migration (Liu et al., 2005; Bergsman et al., 2016), seasonality (Laperrière et al., 2011; Moschini et al., 2017), temperature dependence (Bhowmick et al., 2020, 2023; Marini et al., 2020; Okuneye and Gumel, 2016), two-category avian structure (Abdelrazec et al., 2014; West and Chellamuthu, 2020) and multi-host structure (Ferraguti et al., 2023). No single framework analyses the two avian categories, lateral avian transmission through an explicit environmental reservoir, vertical transmission through the complete mosquito life cycle and the human transfusion and transplantation routes simultaneously under seasonal forcing. That is the gap addressed here. We establish existence, positivity, boundedness and uniqueness of a periodic solution; uniform persistence and the disease-free periodic solution; the periodic reproduction ratio $\mathscr{R}_0^P$ as the spectral radius of the next-infection operator of Wang and Zhao (2008); a bird seeding index; and global asymptotic stability of the endemic periodic solution.

2 Methods

2.1 Model formulation

The model is a deterministic compartmental system of non-linear ordinary differential equations comprising the vector and host populations together with the viral population in the environment. The mosquito, reservoir host (bird) and incidental host (human) populations are

$$N_M = S_E + I_E + S_L + I_L + S_M^F + E_M^F + I_M^F, \tag{1}$$

$$N_B = S_B^C + S_B^N + E_B^C + E_B^N + I_B^C + I_B^N + R_B^C + R_B^N, \qquad N_H = S_H + E_H + I_H^A + I_H^N + I_H^I + R_H. \tag{2}$$

The state variables are defined in Table 1, the parameters in Table 2 and the schematic flow in Figure 1.

Table 1. Modified model variables and their definitions.

Variable	Description	Variable	Description
$S_E(t)$	Susceptible mosquito egg	$R_B^C(t)$	Recovered corvid bird
$I_E(t)$	Infected mosquito egg	$R_B^N(t)$	Recovered non-corvid bird
$S_L(t)$	Susceptible mosquito larvae	$S_H(t)$	Susceptible human
$I_L(t)$	Infected mosquito larvae	$E_H(t)$	Exposed human
$S_M^F(t)$	Susceptible female mosquito	$I_H^A(t)$	Asymptomatic infected human
$E_M^F(t)$	Exposed female mosquito	$I_H^N(t)$	Non-neuroinvasive infected human
$I_M^F(t)$	Infected female mosquito	$I_H^I(t)$	Neuroinvasive infected human
$S_B^C(t)$	Susceptible corvid bird	$R_H(t)$	Recovered human
$S_B^N(t)$	Susceptible non-corvid bird	$D(t)$	WNv contaminated environment
$E_B^C(t)$	Exposed corvid bird	$N_H(t)$	Total human population
$E_B^N(t)$	Exposed non-corvid bird	$N_B(t)$	Total bird population
$I_B^C(t)$	Infected corvid bird	$N_M(t)$	Total mosquito population
$I_B^N(t)$	Infected non-corvid bird		

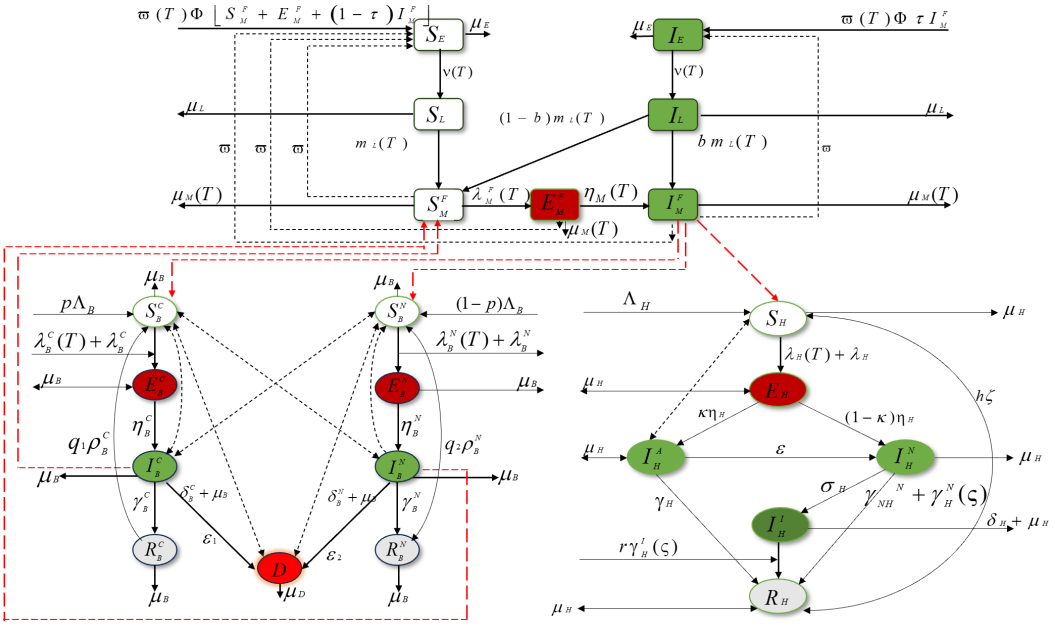

Figure 1. Schematic of the WNv model, showing the mosquito life cycle with vertical transmission (top), the corvid and non-corvid reservoirs with the environmental compartment D (bottom left), and the human population with its three infection outcomes (bottom right).

Susceptible eggs are replenished by $\varpi(T)\Phi[S_M^F + E_M^F + (1-\tau)I_M^F]$ and infected eggs by $\varpi(T)\Phi\tau I_M^F$, both depleted by decay μ_E and hatching $\nu(T)$. Larvae mature into adults at a rate modulated by

$$\Phi = \max\left\{0,\, 1 - \frac{N_L}{K_L}\right\}, \tag{3}$$

with N_L the larval density and K_L the carrying capacity. The traits $\varpi(T), \nu(T), \eta_M(T), \beta(T)$ follow the Brière function and $\mu_M(T)$ the Gaussian formula,

$$f(T) = \begin{cases} cT(T - T_{min})\sqrt{T_{max} - T}, & T_{min} < T < T_{max} \\ 0, & \text{otherwise,} \end{cases} \qquad \mu_M(T) = \mu_{min} \exp\left(\frac{(T - T_{opt})^2}{\sigma_M^2}\right), \tag{4}$$

and the seasonal temperature is $T(t) = \bar{T} + A\cos\left(\frac{2\pi}{365}(t - \phi)\right)$. The abundances are linked by $\alpha_B = N_M^0/N_B^0$ and $\alpha_H = N_M^0/N_H^0$, fixing the blood-meal index $\varphi_F N_B^0 + N_H^0$.

Table 2. Modified model parameters and their descriptions.

Parameter	Description	Parameter	Description
Demographic			
Λ_H	Recruitment rate for human	μ_L	Larva natural mortality rate
Λ_B	Bird recruitment rate	$\mu_M(T)$	Adult mosquito natural mortality rate
μ_H	Human natural death rate	μ_B	Bird natural mortality rate
μ_E	Egg natural decay rate	μ_D	WNv decay rate
Transmission			
β_{1M}	Transmission probability from corvid bird to mosquito	$\varpi(T)$	Temperature-dependent oviposition rate
β_{2M}	Transmission probability from non-corvid bird to mosquito	τ	Vertical transmission rate
β_H	Transmission probability from mosquito to human	a	Fraction of larvae maturing into female adult mosquito
β_B^C	Transmission probability from mosquito to corvid bird	b	Proportion of infected larvae maturing into infected adults
β_B^N	Transmission probability from mosquito to non-corvid bird	p_1	Probability of transmission via blood transfusion
θ_M	Non-diapausing mosquitoes	p_2	Probability of transmission via organ transplant
Disease progression			
η_H	Disease incubation rate in human	κ	Fraction of asymptomatic infected individuals
$\eta_M(T)$	Disease incubation rate in mosquito	ε	Rate of becoming symptomatic from asymptomatic state
η_B^C	Disease incubation rate in corvid bird	δ_H	Disease induced mortality for human
η_B^N	Disease incubation rate in non-corvid bird	δ_B^C	Disease induced mortality for corvids
$\gamma_H^N(\varsigma)$	Recovery rate due to supportive treatment, non-neuroinvasive	δ_B^N	Disease induced mortality for non-corvids
$\gamma_H^I(\varsigma)$	Recovery rate due to supportive treatment, neuroinvasive	ε_1	Corvid bird viral shedding coefficient
γ_B^C	Corvid bird recovery rate	ε_2	Non-corvid bird viral shedding coefficient
γ_B^N	Non-corvid bird recovery rate		
Saturation and recovery			
ξ_1	Recovery rate coefficient, non-neuroinvasive case	γ_H	Natural recovery rate for asymptomatic human
ξ_2	Recovery coefficient, neuroinvasive case	γ_{NH}^N	Natural recovery rate, non-neuroinvasive case
υ_1	Saturation parameter, neuroinvasive case	σ_H	Rate of developing neuroinvasive disease
υ_2	Saturation parameter, non-neuroinvasive case	r	Fraction of neuroinvasive cases recovering due to treatment
Contact and migration			
$\nu(T)$	Mosquito egg hatching rate	y_0^C	Peak introduction for corvid birds

Continued on next page

Table 2 continued from previous page

Parameter	Description	Parameter	Description
$m_L(T)$	Temperature-dependent larval maturation rate	y_0^N	Peak introduction for non-corvid birds
$\beta(T)$	Temperature-dependent mosquito biting rate	y_m	Day of peak introduction
φ_F	Mosquito feeding index	y_w	Width of pulse
Other			
h	Waning immunity rate in human	ϑ_i	Bird predation rate
ζ	Recovery to susceptible	α_B	Ratio of mosquito to bird
p	Fraction of corvids recruited into susceptible class	α_H	Ratio of mosquito to human
b_B	Recruitment rate for birth	π_{ij}	Bird food and water consumption rate
q_i	Fraction of recovered birds losing immunity	K_L	Environmental carrying capacity for larvae
ρ_B^C	Immunity loss rate for corvids	K_{sat}	Half-saturation constant for predation-mediated transmission
ρ_B^N	Immunity loss rate for non-corvids	$\bar{T}$	Mean annual temperature
a_{H1}	Proportion of humans undergoing blood transfusion	T_{max}	Mean annual maximum temperature
a_{H2}	Proportion of humans undergoing organ transplant	T_{min}	Mean annual minimum temperature
d_1	Proportion of predator corvid birds	A	Amplitude
d_2	Proportion of predator non-corvid birds	ϕ	Phase shift

2.2 Model equations

The mosquito subsystem is

$$\begin{cases} \dfrac{dS_E}{dt} = \varpi(T)\Phi\big(S_M^F + E_M^F + (1-\tau)I_M^F\big) - (\nu(T)+\mu_E)S_E \\ \dfrac{dI_E}{dt} = \varpi(T)\Phi\tau I_M^F - (\nu(T)+\mu_E)I_E \\ \dfrac{dS_L}{dt} = \nu(T)S_E - m_L(T)S_L - \mu_L S_L \\ \dfrac{dI_L}{dt} = \nu(T)I_E - (1-b)m_L(T)I_L - bm_L(T)I_L - \mu_L I_L \\ \dfrac{dS_M^F}{dt} = am_L(T)S_L + (1-b)am_L(T)I_L - (\lambda_M^F(T)+\mu_M(T))S_M^F \\ \dfrac{dE_M^F}{dt} = \lambda_M^F(T)S_M^F - (\eta_M(T)+\mu_M(T))E_M^F \\ \dfrac{dI_M^F}{dt} = abm_L(T)I_L + \eta_M(T)E_M^F - \mu_M(T)I_M^F \end{cases} \tag{5}$$

where $\lambda_M^F(T) = \dfrac{(\beta_{1M} I_B^C + \beta_{2M} I_B^N)\beta(T)\theta_M}{\varphi_F N_B + N_H}$. The human subsystem is

$$\begin{cases} \dfrac{dS_H}{dt} = \Lambda_H + h\zeta R_H - (\lambda_H(T) + \tilde{\lambda}_H + \mu_H) S_H \\ \dfrac{dE_H}{dt} = (\lambda_H(T) + \tilde{\lambda}_H) S_H - (\kappa\eta_H + (1-\kappa)\eta_H + \mu_H) E_H \\ \dfrac{dI_H^A}{dt} = \kappa\eta_H E_H - (\varepsilon + \gamma_H + \mu_H) I_H^A \\ \dfrac{dI_H^N}{dt} = (1-\kappa)\eta_H E_H + \varepsilon I_H^A - (\sigma_H + \gamma_{NH}^N + \gamma_H^N(\varsigma) + \mu_H) I_H^N \\ \dfrac{dI_H^I}{dt} = \sigma_H I_H^N - (r\gamma_H^I(\varsigma) + \delta_H + \mu_H) I_H^I \\ \dfrac{dR_H}{dt} = \gamma_H I_H^A + \big(\gamma_{NH}^N + \gamma_H^N(\varsigma)\big) I_H^N + r\gamma_H^I(\varsigma) I_H^I - (h\zeta + \mu_H) R_H \end{cases} \tag{6}$$

where $\lambda_H(T) = \dfrac{\beta_H \beta(T)\theta_M I_M^F}{\varphi_F N_B + N_H}$, $\tilde{\lambda}_H = \big(p_1 a_{H1} + p_2 a_{H2}\big)\frac{I_H^A}{N_H}$, $\gamma_H^N(\varsigma) = \frac{\xi_1 I_H^N}{1+\upsilon_1 I_H^N}$ and $\gamma_H^I(\varsigma) = \frac{\xi_2 I_H^I}{1+\upsilon_2 I_H^I}$. The environmental compartment satisfies

$$\frac{dD}{dt} = (\varepsilon_1 + \delta_B^C + \mu_B) I_B^C + (\varepsilon_2 + \delta_B^N + \mu_B) I_B^N - \mu_D D, \tag{7}$$

and the bird subsystem, with continuous introduction of infected birds, is

$$\begin{cases} \dfrac{dS_B^C}{dt} = p\Lambda_B + q_1\rho_B^C R_B^C - (\lambda_B^C(T) + \tilde{\lambda}_B^C + \mu_B) S_B^C \\ \dfrac{dE_B^C}{dt} = (\lambda_B^C(T) + \tilde{\lambda}_B^C) S_B^C - (\eta_B^C + \mu_B) E_B^C \\ \dfrac{dI_B^C}{dt} = \eta_B^C E_B^C - (\gamma_B^C + \delta_B^C + \mu_B) I_B^C + \psi_B^C(t) \\ \dfrac{dR_B^C}{dt} = \gamma_B^C I_B^C - (q_1\rho_B^C + \mu_B) R_B^C \\ \dfrac{dS_B^N}{dt} = (1-p)\Lambda_B + q_2\rho_B^N R_B^N - (\lambda_B^N(T) + \tilde{\lambda}_B^N + \mu_B) S_B^N \\ \dfrac{dE_B^N}{dt} = (\lambda_B^N(T) + \tilde{\lambda}_B^N) S_B^N - (\eta_B^N + \mu_B) E_B^N \\ \dfrac{dI_B^N}{dt} = \eta_B^N E_B^N - (\gamma_B^N + \delta_B^N + \mu_B) I_B^N + \psi_B^N(t) \\ \dfrac{dR_B^N}{dt} = \gamma_B^N I_B^N - (q_2\rho_B^N + \mu_B) R_B^N \end{cases} \tag{8}$$

where, for $i = 1, 2$ with $1 \equiv C$ and $2 \equiv N$,

$$\lambda_i(T) = \frac{\beta_i \beta(T)\theta_M \varphi_F I_M^F}{\varphi_F N_B + N_H}, \quad \tilde{\lambda}_i = \beta_i \pi_{ij} \frac{D}{N_B} + \frac{I_B^C}{1 + I_B^C/K_{sat}} d_1 \beta_B^C \vartheta_1 + \frac{I_B^N}{1 + I_B^N/K_{sat}} d_2 \beta_B^N \vartheta_2, \tag{9}$$

and the introduction function is

$$\psi_i(t) = y_0 \left(\frac{e^{(y_m - t)/y_w}}{\big(1 + e^{(y_m - t)/y_w}\big)^2} \right). \tag{10}$$

Throughout $\beta_{1M} > \beta_{2M}$, $\beta_1 > \beta_2$ and $\varepsilon_1 > \varepsilon_2$, reflecting the higher viraemia and shedding of corvids (CWHL, 2024). We write $x = (x_1, \ldots, x_{22})^T$ for the state vector of (5)–(8) and $\Gamma = \mathbb{R}_+^{22}$.

2.3 Periodic setting

The functions $\varpi(T(t)), \mu_M(T(t)), \nu(T(t)), \eta_M(T(t)), \beta(T(t)), \psi_B^C(t), \psi_B^N(t)$ are continuous, positive and ω-periodic with $\omega = 365$ days. Write $\dot{x}_i = F_i(t, x) - V_i(t, x)$ with the $m = 13$ infected compartments ordered first, and let $\Phi_A(t, s)$ denote the evolution operator of $\dot{y} = A(t)y$. Assumptions (A1)–(A7) of Wang and Zhao (2008) hold:

non-negativity, ω-periodicity and C^1 dependence of $F_i, V_i^{\pm}$; $x_i = 0 \Rightarrow V_i^- = 0$; $F_i \equiv 0$ for $i > m$; $F_i = V_i^+ = 0$ on the disease-free subspace for $i \le m$; and $\rho(\Phi_M(\omega)) < 1$, $\rho(\Phi_{-V}(\omega)) < 1$.

Lemma 1. *$V(t)$ is lower triangular with diagonal $v_1(t), \dots, v_{13}(t)$, so that $\rho(\Phi_{-V}(\omega, 0)) = \max_i \exp\big(-\int_0^\omega v_i\big)$, and (A7) holds if and only if $\int_0^\omega v_i > 0$ for each i, guaranteed by $\mu_E, \mu_L, \mu_B, \mu_H, \mu_D > 0$ and $\mu_M(T) > 0$.*

Proposition 2. *For $\lambda > 0$ let W_λ solve $dW_\lambda/dt = [\lambda^{-1}F(t) - V(t)]W_\lambda$, $W_\lambda(0) = I_{13}$. Then $\lambda \mapsto \rho(W_\lambda(\omega))$ is continuous and strictly decreasing on $(0, \infty)$, and $\mathscr{R}_0^P$ is the unique root of $\rho(W_\lambda(\omega)) = 1$. When F and V are constant this reduces to $\lambda = \rho(FV^{-1})$, the classical next-generation matrix of van den Driessche and Watmough (2002).*

3 Results

3.1 Existence, positivity and boundedness

Theorem 3 (Mawhin's continuation theorem)**.** *Let L be a Fredholm operator of index zero and $N : X \to Z$ be L-compact on $\bar{\Omega}$, Ω open and bounded. If every solution of $Lx = \lambda Nx$, $\lambda \in (0, 1)$, satisfies $x \notin \partial\Omega$; $QNx \neq 0$ for $x \in \partial\Omega \cap \ker L$; and $\deg(JQN, \Omega \cap \ker L, 0) \neq 0$, then $Lx = Nx$ has a solution in $\operatorname{Dom} L \cap \bar{\Omega}$.*

Lemma 4 (Uniform a priori bounds)**.** *Let $x(t)$ satisfy $Lx = \lambda Nx$ for some $\lambda \in (0, 1)$ and put $\psi_{max} = \max_{[0,\omega]}\{\psi_B^C + \psi_B^N\}$ and $C_1 = \varepsilon_1 + \varepsilon_2 + \delta_B^C + \delta_B^N + 2\mu_B$. Then, independently of λ,*

$$\|N_H\| \le \frac{\Lambda_H}{\mu_H}, \qquad \|N_B\| \le \frac{\Lambda_B + \psi_{max}}{\mu_B}, \qquad \|D\| \le \frac{C_1(\Lambda_B + \psi_{max})}{\mu_B \mu_D}, \tag{11}$$

and the seven mosquito compartments are bounded through the cascade $\bar{N}_M^F \le (\bar{m}_L/\bar{\mu}_M)\bar{N}_L$, $\bar{N}_L \le (\bar{\nu}/\mu_L)\bar{N}_E$ closed by the density-dependent regulation Φ at carrying capacity K_L. Each individual compartment is bounded by the corresponding total.

With Lemma 4 the set $\Omega = \{x : \|x_i\| < M_i + 1\}$ is open and bounded and no solution of $Lx = \lambda Nx$ meets $\partial\Omega$; the remaining hypotheses of Theorem 3 follow from the sign structure of the averaged vector field on $\ker L$, so the system possesses at least one ω-periodic solution.

Theorem 5 (Positive invariance)**.** *$\Gamma = \mathbb{R}_+^{22}$ is positively invariant: on each coordinate hyperplane $\{x_i = 0\}$ the vector field satisfies $dx_i/dt \ge 0$, so the Nagumo theorem (Walter, 2012) applies, the recruitment terms Λ_H, $p\Lambda_B$, $(1-p)\Lambda_B$ and the non-negative introduction terms preventing extinction.*

Theorem 6 (Ultimate boundedness and invariant region)**.** *All solutions starting in Γ enter and remain in the compact absorbing set*

$$\Gamma^* = \Big\{x \in \mathbb{R}_+^{22} : N_H \le \frac{\Lambda_H}{\mu_H},\ N_B \le \frac{\Lambda_B + \psi_{max}}{\mu_B},\ N_M \le N_M^*,\ D \le D^*\Big\}, \tag{12}$$

where $N_M^* = \varpi_{max} K_L/\mu_{M,min}$ and $D^* = C_1 N_B^*/\mu_D$, and Γ^* is positively invariant.

3.2 Persistence and the disease-free periodic solution

Theorem 7 (Uniform persistence)**.** *Assume $\mathscr{R}_0^P > 1$. Then there exists $\varepsilon > 0$ with $\liminf_{t\to\infty} \min_{i\in\mathcal{I}} x_i(t; x_0) \ge \varepsilon$ for all $x_0 \in X^0$, where $\mathcal{I} = \{2, 4, 6, 7, 9, 10, 11, 12, 16, 17, 20, 21\}$.*

Remark 8. Because $\psi_B^C, \psi_B^N > 0$, a true disease-free state does not exist; the disease-free periodic solution is therefore defined for the unforced system, $\psi_i \equiv 0$.

Theorem 9 (Disease-free periodic solution)**.** *When $\psi_B^C \equiv \psi_B^N \equiv 0$ the system admits the unique disease-free periodic solution*

$$x^0(t) = \big(S_{B,0}^C, 0, 0, R_{B,0}^C, S_{B,0}^N, 0, 0, R_{B,0}^N, S_{E,0}(t), 0, S_{L,0}(t), 0, S_{M,0}^F(t), 0, 0, S_{H,0}, 0, 0, 0, 0, 0, 0\big), \tag{13}$$

with $S_{B,0}^C = p\Lambda_B/\mu_B$, $S_{B,0}^N = (1-p)\Lambda_B/\mu_B$, $S_{H,0} = \Lambda_H/\mu_H$, and $(S_E^0, S_L^0, S_{M,0}^F)$ the unique positive ω-periodic

solution of

$$\frac{dS_E}{dt} = \varpi(T)\Phi S_M^F - (\nu(T)+\mu_E)S_E, \quad \frac{dS_L}{dt} = \nu(T)S_E - (am_L(T)+\mu_L)S_L, \quad \frac{dS_M^F}{dt} = am_L(T)S_L - \mu_M(T)S_M^F. \tag{14}$$

Theorem 10 (Persistence with migration forcing)**.** *When $\psi_B^C(t) > 0$ or $\psi_B^N(t) > 0$ the system is uniformly persistent regardless of $\mathscr{R}_0^P$, since $\liminf_{t\to\infty} I_i(t) \geq \bar{\psi}_i/(\gamma_i+\delta_i+\mu_B) > 0$ and the resulting infected birds maintain mosquito and hence human infection.*

3.3 Periodic reproduction ratio

Definition 11. With $\Phi_V(t,s)$ the evolution operator of $\dot{z} = -V(t)z$, the next-infection operator on the space of ω-periodic continuous $\varphi : \mathbb{R} \to \mathbb{R}^{13}$ is

$$(L\varphi)(t) = \int_0^\infty \Phi_V(t, t-a)\, F(t-a)\, \varphi(t-a)\, da, \tag{15}$$

and the periodic reproduction ratio is $\mathscr{R}_0^P = \rho(L)$.

Theorem 12 (Threshold)**.** *Under (A1)–(A7), $\mathscr{R}_0^P - 1$ has the same sign as $\rho(\Phi_{F-V}(\omega,0)) - 1$; hence $x^0(t)$ is locally asymptotically stable if $\mathscr{R}_0^P < 1$ and unstable if $\mathscr{R}_0^P > 1$.*

Ordering the infected compartments as $(E_B^C, I_B^C, E_B^N, I_B^N, I_E, I_L, E_M^F, I_M^F, E_H, I_H^A, I_H^N, I_H^I, D)^T$ and linearising at $x^0(t)$,

$$F(t) = \begin{pmatrix}
0 & l_1 & 0 & l_2 & 0 & 0 & 0 & l_3 & 0 & 0 & 0 & 0 & l_4 \\
0 & 0 & 0 & 0 & 0 & 0 & 0 & 0 & 0 & 0 & 0 & 0 & 0 \\
0 & \tilde{l}_1 & 0 & \tilde{l}_2 & 0 & 0 & 0 & l_5 & 0 & 0 & 0 & 0 & l_6 \\
0 & 0 & 0 & 0 & 0 & 0 & 0 & 0 & 0 & 0 & 0 & 0 & 0 \\
0 & 0 & 0 & 0 & 0 & 0 & 0 & l_7 & 0 & 0 & 0 & 0 & 0 \\
0 & 0 & 0 & 0 & 0 & 0 & 0 & 0 & 0 & 0 & 0 & 0 & 0 \\
0 & l_8 & 0 & l_9 & 0 & 0 & 0 & 0 & 0 & 0 & 0 & 0 & 0 \\
0 & 0 & 0 & 0 & 0 & 0 & 0 & 0 & 0 & 0 & 0 & 0 & 0 \\
0 & 0 & 0 & 0 & 0 & 0 & 0 & l_{10} & 0 & l_{11} & 0 & 0 & 0 \\
0 & 0 & 0 & 0 & 0 & 0 & 0 & 0 & 0 & 0 & 0 & 0 & 0 \\
0 & 0 & 0 & 0 & 0 & 0 & 0 & 0 & 0 & 0 & 0 & 0 & 0 \\
0 & 0 & 0 & 0 & 0 & 0 & 0 & 0 & 0 & 0 & 0 & 0 & 0 \\
0 & 0 & 0 & 0 & 0 & 0 & 0 & 0 & 0 & 0 & 0 & 0 & 0
\end{pmatrix}, \tag{16}$$

with

$$\begin{aligned}
&l_1 = d_1\beta_1\vartheta_1 S_B^{C0}, \quad l_2 = d_2\beta_2\vartheta_2 S_B^{C0}, \quad \tilde{l}_1 = d_1\beta_1\vartheta_1 S_B^{N0}, \quad \tilde{l}_2 = d_2\beta_2\vartheta_2 S_B^{N0}, \quad l_7 = \varpi(T)\Phi\tau, \\
&l_3 = \frac{\beta_1\beta(T)\theta_M\varphi_F}{\varphi_F N_B^0 + N_H^0} S_B^{C0}, \quad l_4 = \frac{\beta_1\pi_{1j} S_B^{C0}}{N_B^0}, \quad l_5 = \frac{\beta_2\beta(T)\theta_M\varphi_F}{\varphi_F N_B^0 + N_H^0} S_B^{N0}, \quad l_6 = \frac{\beta_2\pi_{2j} S_B^{N0}}{N_B^0}, \\
&l_8 = \frac{\beta_{1M}\beta(T)\theta_M\varphi_F}{\varphi_F N_B + N_H} S_M^{F0}, \quad l_9 = \frac{\beta_{2M}\beta(T)\theta_M\varphi_F}{\varphi_F N_B + N_H} S_M^{F0}, \quad l_{10} = \frac{\beta_H\beta(T)\theta_M}{\varphi_F N_B^0 + N_H^0} S_H^0, \quad l_{11} = p_1 a_{H1} + p_2 a_{H2},
\end{aligned} \tag{17}$$

and $V(t)$ block lower triangular,

$$V(t) = \begin{pmatrix} V_B & 0 & 0 & 0 \\ 0 & V_M(t) & 0 & 0 \\ 0 & 0 & V_H & 0 \\ -E_B & 0 & 0 & \mu_D \end{pmatrix}, \qquad E_B = (0, \rho_C, 0, \rho_N), \qquad \begin{aligned} \rho_C &= \varepsilon_1 + \delta_B^C + \mu_B, \\ \rho_N &= \varepsilon_2 + \delta_B^N + \mu_B, \end{aligned} \tag{18}$$

with diagonal $v_1 = \eta_B^C + \mu_B$, $v_2 = \gamma_B^C + \delta_B^C + \mu_B$, $v_3 = \eta_B^N + \mu_B$, $v_4 = \gamma_B^N + \delta_B^N + \mu_B$, $v_5 = \nu(T) + \mu_E$, $v_6 = m_L(T) + \mu_L$, $v_7 = \eta_M(T) + \mu_M(T)$, $v_8 = \mu_M(T)$, $v_9 = \eta_H + \mu_H$, $v_{10} = \varepsilon + \gamma_H + \mu_H$, $v_{11} = 1 + \mu_H$, $v_{12} = \delta_H + \mu_H$, $v_{13} = \mu_D$. Only $V_M(t)$ depends on t. The block $-E_B$ is what renders $V(t)$ lower triangular rather than block diagonal, and is the reason the environmental route is visible to the threshold.

Writing $K_{ij}(t,a) = [F(t)\Phi_V(t,t-a)]_{ij}$ for the next-generation kernel and $P_C = \eta_B^C/(v_1v_2)$, $P_N = \eta_B^N/(v_3v_4)$

for the survival-weighted residence factors, the entries governing avian transmission are

$$\begin{aligned} \int_0^\infty K_{1,1}\,da &= P_C\Big[l_1 + \frac{l_4\rho_C}{\mu_D}\Big], \qquad \int_0^\infty K_{1,3}\,da = P_N\Big[l_2 + \frac{l_4\rho_N}{\mu_D}\Big], \\ \int_0^\infty K_{3,1}\,da &= P_C\Big[\tilde{l}_1 + \frac{l_6\rho_C}{\mu_D}\Big], \qquad \int_0^\infty K_{3,3}\,da = P_N\Big[\tilde{l}_2 + \frac{l_6\rho_N}{\mu_D}\Big], \end{aligned} \tag{19}$$

the first term in each bracket being the predatory and scavenging route and the second the environmental route weighted by the mean residence time μ_D^{-1}, and for the human block

$$\int_0^\infty K_{9,9}\,da = \frac{l_{11}\kappa\eta_H}{v_9 v_{10}} = \mathscr{R}_{0,H}. \tag{20}$$

Proposition 13 (Dimensional reduction)**.** *$F(t)$ has non-zero entries only in the rows $\mathcal{N} = \{1,3,5,7,9\}$, so any eigenvector of K with non-zero eigenvalue is supported on $\mathcal{N}$ and $\rho(K) = \rho(K_{red})$, the principal 5×5 submatrix on $\mathcal{N}$. The same argument applies to L.*

Theorem 14 (Block triangularity)**.** *The reduced kernel is block triangular,*

$$K_{5\times5} = \begin{pmatrix} K_{1,1} & K_{1,3} & K_{1,5} & K_{1,7} & 0 \\ K_{3,1} & K_{3,3} & K_{3,5} & K_{3,7} & 0 \\ 0 & 0 & K_{5,5} & K_{5,7} & 0 \\ K_{7,1} & K_{7,3} & 0 & 0 & 0 \\ 0 & 0 & K_{9,5} & K_{9,7} & K_{9,9} \end{pmatrix} = \begin{pmatrix} A & 0 \\ * & K_{9,9} \end{pmatrix}, \tag{21}$$

since no route leads from a human compartment to a vector or reservoir compartment. Hence

$$\mathscr{R}_0^P = \max\big\{\rho(A),\ \mathscr{R}_{0,H}\big\}, \qquad \mathscr{R}_{0,H} = \frac{\kappa\eta_H(p_1 a_{H1} + p_2 a_{H2})}{(\eta_H+\mu_H)(\varepsilon+\gamma_H+\mu_H)}. \tag{22}$$

Remark 15. No parameter of the human block depends on temperature, so there F and V are constant, Φ_V reduces to a matrix exponential and $\mathscr{R}_{0,H}$ remains exact under seasonal forcing. Only $\rho(A)$ requires numerical treatment.

Proposition 2 was implemented by integrating W_λ over one period with $F(t)$ and $V(t)$ rebuilt from $T(t)$ at every step and locating the root of $\rho(W_\lambda(\omega)) = 1$ by bisection. Table 3 records the threshold with the frozen and time-averaged quantities.

Table 3. Periodic reproduction ratio and the corresponding frozen and time-averaged quantities.

Quantity	Definition	Value
$\mathscr{R}_0^P$	Periodic ratio, root of $\rho(W_\lambda(\omega)) = 1$	1.494471
$\mathscr{R}_0^{(0)}$	Frozen form at period-averaged parameters	1.518752
$\mathscr{R}_0(25.00\,^\circ\mathrm{C})$	Frozen form at the reference temperature	1.858996
$\mathscr{R}_0(34.62\,^\circ\mathrm{C})$	Frozen form at the seasonal maximum	1.057777
$\mathscr{R}_0(20.20\,^\circ\mathrm{C})$	Frozen form at the seasonal minimum	1.081869
Averaging error	$(\mathscr{R}_0^{(0)} - \mathscr{R}_0^P)/\mathscr{R}_0^P$	+1.62%
Freezing error	at the reference temperature	+24.39%

Since $\mathscr{R}_0^P = 1.494471 > 1$ the system is uniformly persistent and the disease-free periodic solution is unstable. Freezing the temperature at 25 °C overstates the threshold by 24.39%, seasonal forcing depressing it by 19.61%: the frozen value at either seasonal extreme falls far below its value at the reference temperature, so the thermal response is unimodal over the annual range and the seasonal excursion carries the system away from the optimum in both directions. Figure 2 shows the instantaneous reproduction number, doubly peaked with a trough at the annual temperature maximum. Exceeding unity throughout the year, it is not a threshold quantity; persistence is governed by $\mathscr{R}_0^P$.

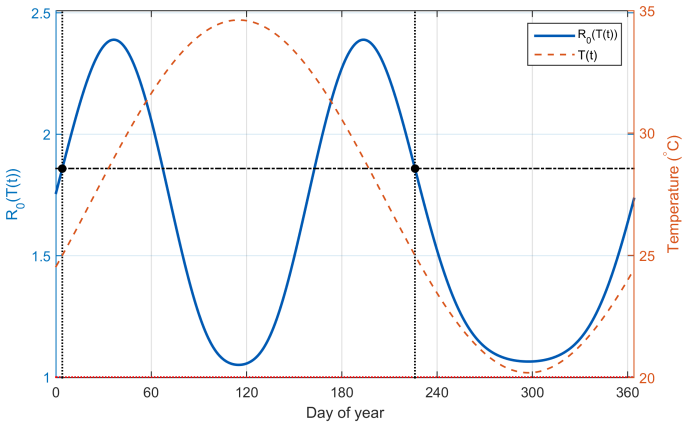

Figure 2. Instantaneous reproduction number $\mathscr{R}_0(T(t))$ (solid) and the annual temperature profile $T(t)$ (dashed) over one period. The dash-dotted line marks the frozen value at the reference temperature and the dotted line the unit threshold.

3.4 Bird seeding index

The introduction $\psi_i(t)$ does not enter the linearisation and so does not affect $\mathscr{R}_0^P$, but it maintains a non-zero infected bird pool. The resulting transmission is quantified by

$$\mathscr{S} = \int_0^\omega \lambda_M^F(t)\,\phi_{8,8}(\omega,t)\,dt = \int_0^\omega \frac{\beta_{iM}\beta(T)\theta_M\varphi_F\tilde{I}_i(t)}{\varphi_F N_B + N_H}\, e^{-\int_t^\omega \mu_M(T(\xi))\,d\xi}\,dt, \tag{23}$$

where $\tilde{I}_i$ is the unique ω-periodic solution of $d\tilde{I}_i/dt = \psi_i(t) - k_i\tilde{I}_i$, with $k_C = \gamma_B^C + \delta_B^C + \mu_B$, $k_N = \gamma_B^N + \delta_B^N + \mu_B$ and

$$\tilde{I}_i(0) = \frac{\int_0^\omega \psi_i(s)e^{-k_i(\omega-s)}\,ds}{1 - e^{-k_i\omega}}. \tag{24}$$

With the values of Tables 3 and 5,

$$\mathscr{S} = 3.35 \times 10^{-8} > 0, \tag{25}$$

so the system remains endemic even when $\mathscr{R}_0^P < 1$.

3.5 The endemic periodic solution

Theorem 16 (Existence and uniqueness)**.** *Assume $\mathscr{R}_0^P > 1$. Then there exists a unique positive ω-periodic solution $x^*(t) \in \mathrm{int}(\mathbb{R}_+^{22})$.*

Proof. The Poincaré map $P(x_0) = x(\omega; x_0)$ maps the compact convex absorbing set of Theorem 6 into itself and is continuous, so Schauder's theorem gives a fixed point x^*, which is an ω-periodic solution. By Theorem 7 it cannot lie in the disease-free set, and positivity of the susceptible compartments follows from the integral representation, the recruitment and introduction terms keeping the integral strictly positive. Uniqueness follows from the implicit function theorem applied to $G(x) = P(x) - x$ on the absorbing set. □

Theorem 17 (Global asymptotic stability)**.** *The endemic periodic solution $x^*(t)$ is globally asymptotically stable on $\mathbb{R}_+^{22}$: its basin of attraction $\mathscr{B}(x^*) = \{x_0 : \lim_{t\to\infty} \|x(t;x_0) - x^*(t)\| = 0\}$ is the whole biologically feasible region.*

Proof. By Theorems 5 and 6 the system is dissipative on a positively invariant orthant; by Theorems 7 and 10 it is uniformly persistent and the continuous introduction precludes a disease-free equilibrium, so all ω-limit sets lie in the interior; and by Theorem 16 the endemic orbit is the unique periodic solution there. A dissipative, uniformly persistent periodic system with a unique interior periodic orbit and no boundary attractor admits no other ω-limit set, so every bounded trajectory converges to $x^*(t)$. □

The hypotheses were verified numerically by Monte Carlo basin estimation following Schultz et al. (2017): 150 initial conditions drawn from the feasible region, proportional perturbations $c \in \{1.5, 2, 3, 5\}$, tripling of each

of the six biological subsystems in turn, a search for alternative attractors from 100 diverse initial conditions, and five outbreak scenarios up to twenty-fold, all integrated with `ode15s` over 3650 days at relative tolerance 10^{-5}. All 150 trajectories converged, with mean convergence time 39.8 days, mean final relative distance 2.56% and mean periodicity error 0.33%; every proportional and compartment-specific perturbation converged; the attractor search detected exactly one periodic orbit of period 365 days, confirming uniqueness; and all outbreak scenarios recovered within six months (Figure 3).

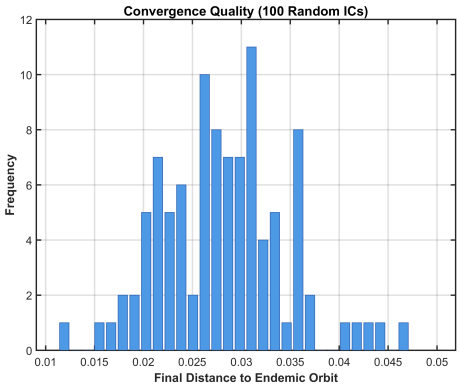

(a) Convergence quality to periodic orbit

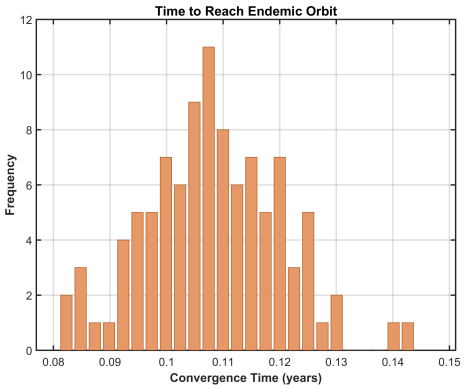

(b) Time for convergence

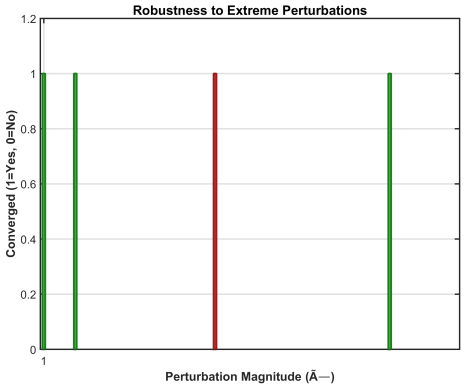

(c) Robustness to convergence

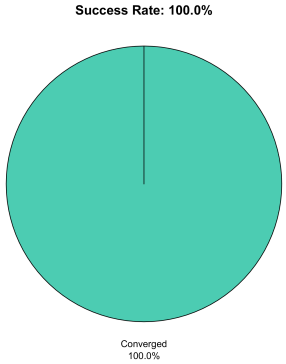

(d) Convergence success rate

Figure 3. Monte Carlo verification of the basin of attraction from 150 random initial conditions spanning the biologically feasible region.

The four panels of Figure 3 record the outcome. The final distances in panel (a) form a single cluster between 0.012 and 0.047 with a mode near 0.030, every sample lying an order of magnitude below the 15% convergence criterion, so no trajectory is marginal and the basin contains no region of slow escape. The convergence times in panel (b) are approximately symmetric about 0.107 years, spanning 0.08 to 0.143 years, that is 29 to 52 days, with only two samples in the upper tail; the absence of a long tail indicates that no part of the sampled region lies near a repelling set, and the whole distribution sits well inside a single annual cycle, so convergence is complete before seasonal forcing has repeated. Panel (c) records the binary outcome for the extreme perturbations of Tests 2 and 5: every bar stands at unity, so recovery does not degrade as the displacement from the orbit grows, and even the twenty-fold environmental and multi-species perturbations return to the orbit. Panel (d) summarises the whole sample as a single sector at 100%. Taken together the panels show a basin that covers the feasible region, is topologically simple, and has no directional escape route.

4 Numerical simulation

The full system was integrated with the data of Tables 4 and 5 until the transients had decayed. The final annual cycle of each population group is displayed in Figure 4 and the aggregate burden and Poincaré convergence in Figure 5.

Table 4. Modified model variables, values, and source.

Variable	Value	Variable	Value
$S_E(0)$	8.28×10^7 (Assumed)	$E_B^N(0)$	0 (Pawelek et al., 2014)
$I_E(0)$	0 (Pawelek et al., 2014)	$I_B^N(0)$	0 (Pawelek et al., 2014)
$S_L(0)$	1.21×10^8 (Assumed)	$R_B^N(0)$	0 (Pawelek et al., 2014)
$I_L(0)$	0 (Pawelek et al., 2014)	$S_H(0)$	3.06×10^7 (National Bureau of Statistics, 2026)
$S_M^F(0)$	7.86×10^8 (Assumed)	$E_H(0)$	0 (Pawelek et al., 2014)
$E_M^F(0)$	0 (Pawelek et al., 2014)	$I_H^A(0)$	0 (Pawelek et al., 2014)
$I_M^F(0)$	0 (Pawelek et al., 2014)	$I_H^N(0)$	0 (Pawelek et al., 2014)
$S_B^C(0)$	7.66×10^6 (Assumed)	$I_H^I(0)$	0 (Pawelek et al., 2014)
$E_B^C(0)$	0 (Assumed)	$R_H(0)$	0 (Pawelek et al., 2014)
$I_B^C(0)$	0 (Pawelek et al., 2014)	$D(0)$	0 (Assumed)
$R_B^C(0)$	0 (Pawelek et al., 2014)	$S_B^N(0)$	— (Assumed)

Table 5. Model parameter values used for the numerical simulation.

Parameter	Baseline	Range	Source
Demographic			
Λ_H	1072 day^{-1}	–	Calculated
Λ_B	$0.000365N_B$ day^{-1}	–	Assumed
$\varpi(T)$	33.8 day^{-1}	Varies	Marini et al. (2020)
μ_H	3.91×10^{-5} day^{-1}	(1.96×10^{-5})	Sweilam et al. (2019)
μ_E	0.125 day^{-1}	(0.0625–0.1875)	Assumed
μ_L	0.1041 day^{-1}	0.071–0.25	Okuneye and Gumel (2016)
$\mu_M(T)$	0.0595 day^{-1}	Varies	Okuneye and Gumel (2016)
μ_B	0.000365 day^{-1}	–	Calculated from Mbaoma et al. (2024)
μ_D	0.55 day^{-1}	(0.1–1.0)	Assumed
Transmission			
β_{1M}	0.70	(0–1)	Bhowmick et al. (2020)
β_{2M}	0.50	(0–1)	Bhowmick et al. (2020)
β_H	0.01	–	Abdelrazec et al. (2014)
β_B^C	0.5601	–	Laine (2014)
β_B^N	0.4	(0.088–0.9)	Abdelrazec et al. (2015)
θ_M	$f(D_M)$	–	Bhowmick et al. (2023)
τ	0.5	(0–1.0)	Nelms et al. (2013)
a	0.9	(0.8–1.0)	Assumed
b	0.1	(0.05–0.15)	Baqar et al. (1993)
p_1	0.05	(0–0.1)	Assumed
p_2	0.1	(0–0.25)	Assumed
Disease progression			
η_H	0.10 day^{-1}	–	Abdelrazec et al. (2014)
$\eta_M(T)$	0.0469 day^{-1}	Varies	Laine (2014)
η_B^C	0.33 day^{-1}	–	Laine (2014)
η_B^N	0.25 day^{-1}	–	Laine (2014)
κ	0.75	–	West and Chellamuthu (2020); CDC (2019)
ε	0.1 day^{-1}	(0.05–0.15)	Assumed
δ_H	0.015 day^{-1}	–	Abdelrazec et al. (2015)
δ_B^C	0.50 day^{-1}	(0–0.5)	Moschini et al. (2017)
δ_B^N	0.3 day^{-1}	(0–0.5)	Moschini et al. (2017); Abdelrazec et al. (2015)

Continued on next page

Table 5 continued from previous page

Parameter	Baseline	Range	Source
ε_1	1	–	Calculated from CDC (2003)
ε_2	0.63	–	Calculated from CDC (2003)
Saturation and recovery			
ξ_1	0.225	–	Assumed
ξ_2	0.0675	–	Assumed
υ_1	0.25	–	Assumed
υ_2	0.081	–	Assumed
γ_H	0.00002 day^{-1}	–	Assumed
γ_{NH}^N	0.0714 day^{-1}	–	West and Chellamuthu (2020)
$\gamma_H^N(\varsigma)$	0.5 day^{-1}	Variable	Calculated
$\gamma_H^I(\varsigma)$	0.1 day^{-1}	Variable	Calculated
γ_B^C	0.05 day^{-1}	(0–0.01)	Abdelrazec et al. (2014)
γ_B^N	0.1 day^{-1}	0–0.2	Abdelrazec et al. (2014)
σ_H	0.004	–	Assumed
r	0.80	–	Assumed
Contact and migration			
$\nu(T)$	$2.2 \times 10^{-3} T^{1.77}$	Varies	Marini et al. (2020)
$m_L(T)$	0.343	Varies	Okuneye and Gumel (2016)
$\beta(T)$	0.122	Varies	Mordecai et al. (2019)
φ_F	5	–	Bhowmick et al. (2023)
y_0^C	5 day^{-1}	(0–10)	Bhowmick et al. (2023)
y_0^N	10 day^{-1}	(0–20)	Bhowmick et al. (2023)
y_m	182.5 day	–	Assumed
y_w	30	–	Assumed
Other			
h	0.1	–	Assumed
ζ	0.002 day^{-1}	–	Assumed
p	0.20	–	Assumed
q_i	Varies	–	West and Chellamuthu (2020)
ρ_B^C	0.07 day^{-1}	–	West and Chellamuthu (2020)
ρ_B^N	0.03 day^{-1}	–	West and Chellamuthu (2020)
a_{H1}	0.00004 day^{-1}	–	Estimated from WHO (2026)
a_{H2}	0.00216 day^{-1}	(0.00185–0.00247)	Estimated from WHO (2024)
d_1	0.85	–	Assumed
d_2	0.35	–	Assumed
ϑ_i	1×10^{-4} $\text{bird}^{-1}\text{day}^{-1}$	(0–0.5)	Assumed
α_B	20	(10–30)	Bhowmick et al. (2020)
α_H	0.3	–	Ruktanonchai et al. (2016)
π_{ij}	0.52 day^{-1}	(0.04–1)	Calculated from CornellLab (n.d.)
K_L	1.2175×10^8	Varies	Calibrated from $S_M^{F0} = N_M^0$
K_{sat}	$0.05N_B^0$	$(0.01–0.50)N_B^0$	Assumed; form after Capasso and Serio (1978)

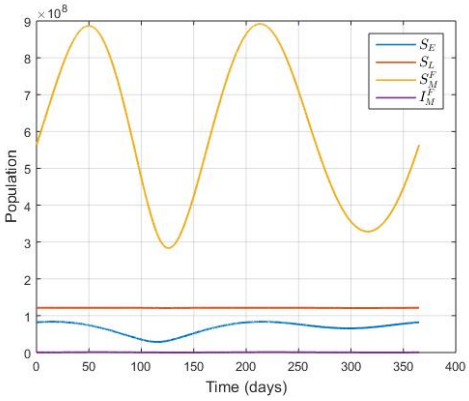

(a) Final annual mosquito periodic orbit

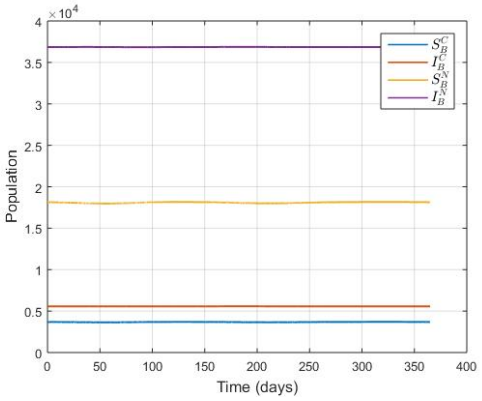

(b) Final annual bird periodic orbit

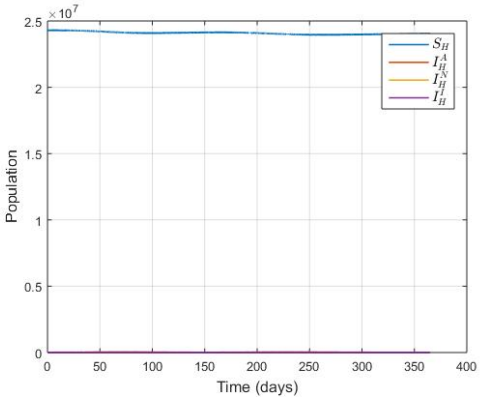

(c) Final annual human periodic orbit

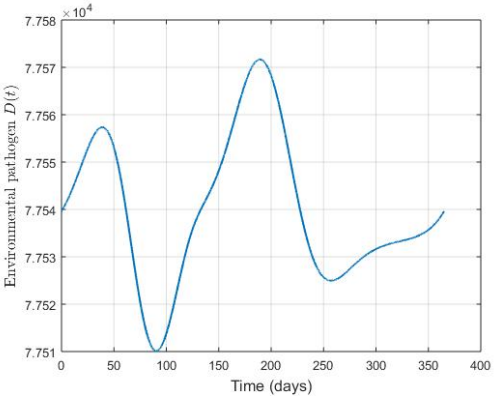

(d) Final annual environmental periodic orbit

Figure 4. Converged annual periodic orbits of the four population groups over one period $\omega = 365$ days.

All compartments return to their initial values after one period, remain strictly positive and stay within the invariant region, as Theorems 3, 5 and 6 require. In Figure 4(a) the susceptible adult female class carries the largest excursion, rising from about 5.7×10^8 to a maximum near 8.9×10^8 around day 50, falling to 2.9×10^8 near day 120 and recovering to a second maximum near day 215; the profile is doubly peaked with a deep trough at the hottest part of the year, the signature of the unimodal thermal response, while the larval class remains near 1.2×10^8, pinned by Φ at K_L. The reservoir classes in Figure 4(b) are essentially flat, at about 3.68×10^4 for I_B^N and 5.5×10^3 for I_B^C: the bird block is autonomous, avian mortality is small relative to the annual frequency, and the introduction function maintains a non-zero infected pool. That I_B^N exceeds I_B^C despite the higher competence of corvids follows from the mortality differential $\delta_B^C = 0.50$ against $\delta_B^N = 0.3$ day^{-1}. In Figure 4(c) the susceptible human class declines gently from 2.43×10^7 to 2.40×10^7 while the infected classes are indistinguishable from zero, the numerical counterpart of Theorem 14. The environmental pathogen in Figure 4(d) oscillates by less than 0.1% about 7.75×10^4, driven by nearly constant shedding and removed at the fast rate $\mu_D = 0.55$ day^{-1}.

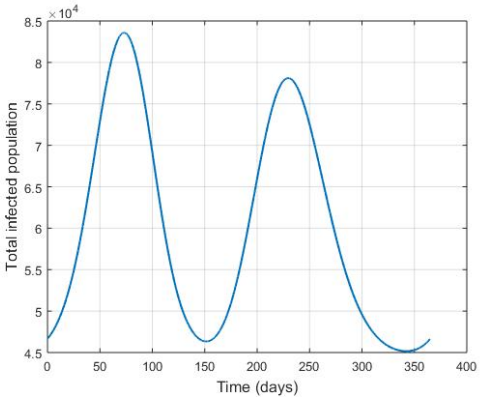

(a) Endemic periodic infection burden

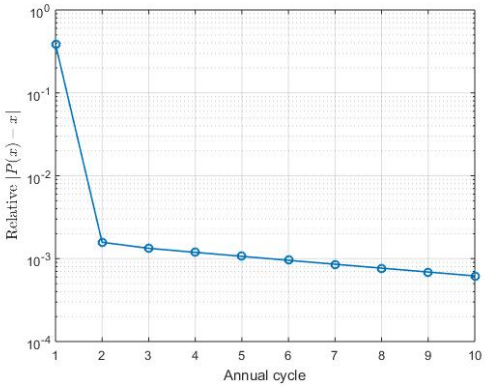

(b) Convergence of the Poincaré map

Figure 5. Aggregate infection burden over the converged annual cycle and the relative displacement $|P(x) - x|$ of the Poincaré map across ten successive annual cycles.

The aggregate burden in Figure 5(a) rises from about 4.65×10^4 to a maximum of 8.35×10^4 near day 72, falls to 4.65×10^4 near day 150, rises to a second maximum of 7.8×10^4 near day 230 and declines to an annual minimum near day 345. It closes exactly on its initial value, so it is the endemic periodic solution of Theorem 16; it never approaches zero, the minimum being some 55% of the maximum, consistent with uniform persistence and the seeding mechanism; and the two peaks straddle the annual temperature maximum rather than coinciding with it, the lag being the accumulated latent and maturation delays. Figure 5(b) shows the relative displacement of the Poincaré map falling from about 4×10^{-1} after the first cycle to 1.6×10^{-3} after the second and 6×10^{-4} by the tenth, decaying monotonically with no plateau, which confirms that the fixed point of P is attracting and that no competing attractor is present.

5 Discussion

The analysis separates into a structural part, which is exact, and an evaluative part, which is numerical, the boundary being drawn by temperature dependence. The bird, human and environmental blocks of $V(t)$ carry no temperature-dependent rate, so there the evolution operator reduces to a matrix exponential and the kernel entries, P_C, P_N and $\mathscr{R}_{0,H}$, are elementary. On the vector block $V_M(t)$ and $V_M(t')$ do not commute for $t \neq t'$, the survivorship kernels admit no elementary antiderivative under a Brière or Gaussian response with sinusoidal forcing, and the threshold must be located by root-finding.

Three findings carry epidemiological weight. First, evaluating the closed-form reproduction number at a fixed 25 °C overstates the periodic threshold by 24.39%, whereas period-averaged parameters err by only 1.62%; both are biased upward because the thermal response is concave near its optimum, so by Jensen's inequality the average of the function lies below the function of the average. Constant-temperature assessments of invasion risk in tropical settings therefore overstate the threshold systematically. Second, the sub-diagonal block $-E_B$ is what makes the environmental route visible to the threshold, the bracketed structure $[l_1 + l_4\rho_C/\mu_D]$ separating the predatory and scavenging route from the environmental route weighted by μ_D^{-1}; both bypass the vector entirely and are absent from the classical mosquito–bird formulations of Wonham et al. (2004), Cruz-Pacheco et al. (2005) and Bowman et al. (2005). Third, the introduction function does not affect $\mathscr{R}_0^P$, yet the positive seeding index $\mathscr{S} = 3.35 \times 10^{-8}$ shows that transmission is maintained even when $\mathscr{R}_0^P < 1$: control effort directed at reducing $\mathscr{R}_0^P$ below unity will not by itself eliminate transmission where reintroduction by migratory or transported birds is continual.

Several limitations should be noted. Uniqueness rests on a sufficient condition verified through a parameter inequality rather than derived from first principles; global stability rests on Monte Carlo basin estimation rather than a constructed global Lyapunov functional; and a number of parameters in Table 5 are assumed rather than estimated from field data.

6 Conclusion

A twenty-two compartment, seasonally forced model of West Nile virus transmission incorporating two avian categories, lateral transmission by predation, scavenging and an environmental reservoir, vertical transmission through the complete mosquito life cycle, and the transfusion and transplantation routes in humans has been analysed. Existence of a positive ω-periodic solution was established by Mawhin's continuation theorem after uniform a priori bounds were derived for every compartment; the non-negative orthant is positively invariant, the periodic solution strictly positive, and all solutions ultimately bounded within a compact absorbing set on which the periodic solution is unique. The system is uniformly persistent, and a unique disease-free periodic solution exists once the avian introduction terms are set to zero. The periodic reproduction ratio was obtained as the spectral radius of the next-infection operator, the thirteen-dimensional kernel being reduced to a five-dimensional block-triangular matrix separating an autonomous human block from a temperature-driven vector-reservoir block, and evaluated at $\mathscr{R}_0^P = 1.494471$, some 19.61% below the constant-temperature value. A positive bird seeding index $\mathscr{S} = 3.35 \times 10^{-8}$ shows that transmission persists even below threshold, and the endemic periodic solution is unique and globally asymptotically stable on the biologically feasible region. The contribution to development is a framework in which the temperature-driven and temperature-independent components of the threshold are separated exactly, and in which reintroduction is shown to sustain endemicity independently of the threshold itself.

Availability of data and material

All data supporting the findings of this study are contained within the article.

Competing Interest

No competing interest is hereby declared by the authors.

Funding

This research received no specific grant from any funding agency in the public, commercial or not-for-profit sectors.

Acknowledgments

The authors thank the Department of Mathematics, Faculty of Physical Sciences, Modibbo Adama University, Yola, for institutional support during the conduct of this research.

Authors' information

[1]Department of Mathematics, Faculty of Physical Sciences, Modibbo Adama University, Yola, Adamawa State, Nigeria.

References

Abdelrazec, A., Lenhart, S., & Zhu, H. (2014). Transmission dynamics of West Nile virus in mosquito and corvids and non-corvids. *Journal of Mathematical Biology*, 68, 1553–1582.

Abdelrazec, A., Lenhart, S., & Zhu, H. (2015). Dynamics and optimal control of a West Nile virus model with seasonality. *Canadian Applied Mathematics Quarterly*, 23(4), 12–33.

Anderson, J. F., Main, A. J., Delroux, K., & Fikrig, E. (2014). Extrinsic incubation periods for horizontal and vertical transmission of West Nile virus by *Culex pipiens* (Diptera: Culicidae). *Journal of Medical Entomology*, 45(3), 445–451.

Baqar, S., Hayes, C. G., Murphy, J. R., & Watts, D. M. (1993). Vertical transmission of West Nile virus by *Culex* and *Aedes* species mosquitoes. *American Journal of Tropical Medicine and Hygiene*, 48(6), 757–762.

Bergsman, L. D., Hyman, J. M., & Manore, C. A. (2016). A mathematical model for the spread of West Nile virus in migratory and resident birds. *Mathematical Biosciences and Engineering*, 13(2), 401–424.

Bhowmick, S., Gethmann, J., Conraths, F. J., Sokolov, I. M., & Lentz, H. H. (2020). Locally temperature-driven mathematical model of West Nile virus spread in Germany. *Journal of Theoretical Biology*, 488, 110117.

Bhowmick, S., Gethmann, J., Conraths, F. J., Sokolov, I. M., & Lentz, H. H. (2023). SEIR-metapopulation model of potential spread of West Nile virus. *Ecological Modelling*, 476, 110213.

Blayneh, K., Gumel, A., Lenhart, S., & Clayton, T. (2010). Backward bifurcation and optimal control in transmission dynamics of West Nile virus. *Bulletin of Mathematical Biology*, 67(5), 1006–1028.

Bowman, C., Gumel, A., van den Driessche, P., Wu, J., & Zhu, H. (2005). A mathematical model for assessing control strategies against West Nile virus. *Bulletin of Mathematical Biology*, 67(5), 1107–1133.

Capasso, V., & Serio, G. (1978). A generalization of the Kermack–McKendrick deterministic epidemic model. *Mathematical Biosciences*, 42(1–2), 43–61.

Centers for Disease Control and Prevention (CDC) (2003). Experimental infection of North American birds with the New York 1999 strain of West Nile virus. *Emerging Infectious Diseases*.

Centers for Disease Control and Prevention (CDC) (2019). West Nile virus.

Centers for Disease Control and Prevention (CDC) (2024c). West Nile virus: Historic data (1999–2023).

Centers for Disease Control and Prevention (CDC) (2024d). West Nile virus and organ transplantation.

Centers for Disease Control and Prevention (CDC) (2024e). West Nile virus: Guidelines for West Nile virus surveillance and control.

Chatterjee, S., Pal, S., & Chattopadhyay, J. (2008). Role of migratory birds under environmental fluctuation: A mathematical study. *Journal of Biological Systems*, 16, 81–106.

Ciota, A. T., & Kramer, L. D. (2013). Vector–virus interactions and transmission dynamics of West Nile virus. *Viruses*, 5, 3021–3047.

Ciota, A. T., Matacchiero, A. C., Kilpatrick, A. M., & Kramer, L. D. (2014). The effect of temperature on life history traits of *Culex* mosquitoes. *Journal of Medical Entomology*, 51(1), 55–62.

Clark, M. B., & Schaefer, T. J. (2023). West Nile virus: Continuing education activity; Etiology.

CornellLab (n.d.). How much do birds eat each day? All About Birds.

Cornell Wildlife Health Lab (CWHL) (2024). West Nile virus: Disease fact sheet.

Cruz-Pacheco, G., Esteva, L., Montaño-Hirose, J. A., & Vargas, C. (2005). Modelling the dynamics of West Nile virus. *Bulletin of Mathematical Biology*, 67, 1157–1172.

Dohm, D. J., Sardelis, M. R., & Turell, M. J. (2002). Experimental vertical transmission of West Nile virus by *Culex pipiens* (Diptera: Culicidae). *Journal of Medical Entomology*, 39(4), 640–644.

European Centre for Disease Prevention and Control (ECDPC) (2025). West Nile virus season in full swing in Europe.

Ferraguti, M., Martins, A. D., & Artzy-Randrup, Y. (2023). Quantifying the invasion risk of West Nile virus: Insights from a multi-vector and multi-host SEIR model. *One Health*, 17, 100638.

García-Carrasco, J. M., Muñoz, A. R., Olivero, J., Segura, M., & Real, R. (2022). Mapping the risk for West Nile virus transmission, Africa. *Emerging Infectious Diseases*, 28(4), 777–785.

Habarugira, G., Suen, W. W., Hobson-Peters, J., Hall, R. A., & Bielefeldt-Ohmann, H. (2020). West Nile virus: An update on pathobiology, epidemiology, diagnostics, control and "one health" implications. *Pathogens*, 9(7), 589.

Heidecke, J., Wallin, J., Fransson, P., Singh, P., Sjödin, H., Stiles, P. C., Treskova, M., & Rocklöv, J. (2025). Uncovering temperature sensitivity of West Nile virus transmission: Novel computational approaches to mosquito-pathogen trait responses. *PLoS Computational Biology*, 21(3), e1012866.

Hinckley, A. F., O'Leary, D. R., & Hayes, E. B. (2007). Transmission of West Nile virus through human breast milk seems to be rare. *Pediatrics*, 119(3), e666–e671.

Jimenez, R. G. C., Lieshout-Krikke, R. W., & Janssen, M. P. (2021). West Nile virus and blood transfusion safety: A European perspective. *Vox Sanguinis*.

Komar, N., Langevin, S., Hinten, S., Nemeth, N., Edwards, E., et al. (2003). Experimental infection of North American birds with the New York 1999 strain of West Nile virus. *Emerging Infectious Diseases*, 9(3), 311–322.

Kramer, L. D., Li, J., & Shi, P.-Y. (2007). West Nile virus. *The Lancet Neurology*, 6(2), 171–181.

Kumar, D., Prasad, G. V., Zaltzman, J., Levy, G. A., & Humar, A. (2004). Community-acquired West Nile virus infection in solid-organ transplant recipients. *Transplantation*, 77(3), 399–402.

Kusne, S., & Smilack, J. (2005). Transmission of West Nile virus by organ transplantation. *Liver Transplantation*, 11(2), 239–241.

Laine, C. G. (2014). *Mathematical modeling the zoonotic and vector transmission dynamics of West Nile virus as they relate to human morbidity and mortality* [Unpublished doctoral dissertation]. Texas A&M University.

Laperrière, V., Brugger, K., & Rubel, F. (2011). Simulation of the seasonal cycles of bird, equine and human West Nile virus cases. *Preventive Veterinary Medicine*, 98(2), 99–110.

Liu, R., Shuai, J., Wu, J., & Zhu, H. (2005). Modeling spatial spread of West Nile virus and impact of directional dispersal of birds. *Mathematical Biosciences and Engineering*, 3(1), 145–160.

Marini, G., Calzolari, M., Angelini, P., Bellini, R., Bellini, S., Bolzoni, L., Torri, D., Defilippo, F., Dorigatti, I., Nikolay, B., Pugliese, A., Rosa, R., & Tamba, M. (2020). A quantitative comparison of West Nile virus incidence from 2013 to 2018 in Emilia-Romagna, Italy. *PLoS Neglected Tropical Diseases*, 14(1), e0007953.

Mbaoma, O. C., Thomas, S. M., & Beierkuhnlein, C. (2024). Spatiotemporally explicit epidemic model for West Nile virus outbreak in Germany: An inversely calibrated approach. *Journal of Epidemiology and Global Health*, 14, 1052–1070.

Miller, B. R., Nasci, R. S., Godsey, M. S., Savage, H. M., Lutwama, J. J., & Lanciotti, R. S. (2000). First field evidence for natural vertical transmission of West Nile virus in *Culex univittatus* complex mosquitoes from Rift Valley Province, Kenya. *American Journal of Tropical Medicine and Hygiene*, 62, 240–246.

Mordecai, E. A., Caldwell, J. M., Grossman, M. K., Lippi, C. A., Johnson, L. R., Neira, M., Rohr, J. R., Ryan, S. J., Savage, V., Shocket, M. S., Sippy, R., Stewart Ibarra, A. M., Thomas, M. B., & Villena, O. (2019). Thermal biology of mosquito-borne disease. *Ecology Letters*, 22, 1690–1708.

Moschini, P., Bisanzio, D., Pugliese, A., & Poletti, P. (2017). A model for the interaction of West Nile virus with seasonal effect in *Culex pipiens* mosquitoes. *Journal of Theoretical Biology*, 430, 45–49.

National Bureau of Statistics (2026). Population 2006–2016.

National Park Service (NPS), US Department of the Interior (2025). West Nile virus: One health.

Nelms, B. M., Fechter-Leggett, E., Carroll, B. D., Macedo, P., Kluh, S., & Reisen, W. K. (2013). Experimental and natural vertical transmission of West Nile virus by California *Culex* (Diptera: Culicidae) mosquitoes. *Journal of Medical Entomology*, 50(2), 371–378.

Nemeth, N. M., & Kunkel, M. R. (2024). West Nile virus in birds. *MSD Veterinary Manual*.

Okuneye, K., & Gumel, A. B. (2016). Analysis of a temperature- and rainfall-dependent model for malaria transmission dynamics. *Mathematical Biosciences*, 287, 72–92.

Pawelek, K. A., Niehaus, P., Salmeron, C., Hager, E. J., & Hunt, G. J. (2014). Modeling dynamics of *Culex pipiens* complex populations and assessing abatement strategies for West Nile virus. *PLoS ONE*, 9(9), e108452.

Powell, J. R., & Tabachnick, W. J. (2013). History of domestication and spread of *Aedes aegypti* — a review. *Memórias do Instituto Oswaldo Cruz*, 108(Suppl. 1), 11–17.

Ronka, S. E., Ruff, J. C., & Murray, K. O. (2021). A 20-year historical review of West Nile virus since its initial emergence in North America: Has West Nile virus become a neglected tropical disease? *PLoS Neglected Tropical Diseases*.

Ruktanonchai, N. W., DeLeenheer, P., Tatem, A. J., Alegana, V. A., Caughlin, T. T., zu Erbach-Schoenberg, E., Lourenco, C., Ruktanonchai, C. W., & Smith, D. (2016). Identifying malaria transmission foci for elimination using human mobility data. *PLoS Computational Biology*, 12(4), e1004846.

Schultz, P., Menck, P. J., Heitzig, J., & Kurths, J. (2017). Potentials and limits to basin stability estimation. *New Journal of Physics*, 19, 023005.

Smithburn, K. C., Hughes, T. P., Burke, A. W., & Paul, J. H. (1940). A neurotropic virus isolated from the blood of a native of Uganda. *The American Journal of Tropical Medicine and Hygiene*, s1-20(4), 471–492.

Stobierski, M. G., Stoltman, G., Downes, F., & Smith, K. (2002). Possible West Nile virus transmission to an infant through breast-feeding — Michigan, 2002. *Morbidity and Mortality Weekly Report*, 51(39), 877–878.

Sule, W. F., Oluwayelu, D. O., Hernandez-Triana, L. M., Fooks, A. R., Venter, M., & Johnson, N. (2018). Epidemiology and ecology of West Nile virus in sub-Saharan Africa. *Parasites & Vectors*, 11, 414.

Sweilam, N. H., Saad, O. M., & Mohamed, D. G. (2019). Fractional optimal control in transmission dynamics of West Nile virus model with state and control time delay: A numerical approach. *Advances in Difference Equations*, 2019, 210.

van den Driessche, P., & Watmough, J. (2002). Reproduction numbers and sub-threshold endemic equilibria for compartmental models of disease transmission. *Mathematical Biosciences*, 180, 29–48.

Walter, W. (2012). *Differential and integral inequalities* (Vol. 55). Springer Science & Business Media.

Wang, W., & Zhao, X.-Q. (2008). Threshold dynamics for compartmental epidemic models in periodic environments. *Journal of Dynamics and Differential Equations*, 20(3), 699–717.

West, N., & Chellamuthu, V. K. (2020). Modeling the effects of passive immunity in birds for the disease dynamics of West Nile virus. *Spora: A Journal of Biomathematics*, 6, 16–25.

Wonham, M. J., de Camino-Beck, T., & Lewis, M. (2004). An epidemiological model for West Nile virus: Invasion analysis and control application. *Proceedings of the Royal Society of London B*, 271, 501–507.

World Health Organization (WHO) (2017). West Nile virus.

World Health Organization (WHO) (2024). Seventy-seventh World Health Assembly — Daily update.

World Health Organization (WHO) (2026). Blood transfusion safety.

World Organisation for Animal Health (WOAH) (2024). West Nile virus: Transmission and spread.